

A Blue Tilt in the Globular Cluster System of the Milky Way-like Galaxy NGC 5170

Duncan A. Forbes^{1*}, Lee R. Spitler¹, W. E. Harris², Jeremy Bailin², Jay Strader^{3*†}, Jean P. Brodie⁴, S. S. Larsen⁵

¹Centre for Astrophysics & Supercomputing, Swinburne University, Hawthorn VIC 3122, Australia

²Department of Physics and Astronomy, McMaster University, Hamilton ON, L8S 4M1, Canada

³Harvard-Smithsonian Centre for Astrophysics, Cambridge, MA 02138, USA

⁴UCO/Lick Observatory, Santa Cruz, CA 95064, USA

⁵Astronomical Institute, Utrecht University, Utrecht, N-3584, The Netherlands

26 October 2018

ABSTRACT

Here we present HST/ACS imaging, in the B and I bands, of the edge-on Sb/Sc galaxy NGC 5170. Excluding the central disk region, we detect a 142 objects with colours and sizes typical of globular clusters (GCs). Our main result is the discovery of a ‘blue tilt’ (a mass-metallicity relation), at the 3σ level, in the metal-poor GC subpopulation of this Milky Way like galaxy. The tilt is consistent with that seen in massive elliptical galaxies and with the self enrichment model of Bailin & Harris. For a linear mass-metallicity relation, the tilt has the form $Z \sim L^{0.42 \pm 0.13}$. We derive a total GC system population of 600 ± 100 , making it much richer than the Milky Way. However when this number is normalised by the host galaxy luminosity or stellar mass it is similar to that of M31. Finally, we report the presence of a potential Ultra Compact Dwarf of size ~ 6 pc and luminosity $M_I \sim -12.5$, assuming it is physically associated with NGC 5170.

Key words: globular clusters: general – galaxies:star clusters – galaxies: individual (NGC 5170)

1 INTRODUCTION

Studies of the globular cluster (GC) system of the Milky Way have benefited from the wealth of information that is available. However such studies are also fundamentally limited by the small sample size of about 150 objects. Discerning more subtle trends in GC properties, or finding GCs in more extreme astrophysical states, requires larger samples which can only be found in the GC systems of other galaxies.

One such trend which was revealed first in extragalactic GC systems, and not seen in the Milky Way GC system, is the so-called ‘blue tilt’. The blue tilt (a trend for the blue GC subpopulation to have redder colours at brighter magnitudes) has been found using the Advanced Camera for Surveys (ACS) on the *Hubble Space Telescope* (HST) in a variety of galaxies from the most massive ellipticals (Harris et al. 2006), to lower mass ellipticals (Strader et al. 2006) and even dwarfs (Mieske et al. 2006a). It has also been detected in an early-type spiral galaxy, the Sombrero, by Spitler et al. (2006). It has not been detected in any HST study of late-

type spirals, but the few studies to date (e.g. Goudfrooij et al. 2003) have generally used the WFPC2 camera which has a more limited field-of-view compared to the ACS camera and hence such studies have focused on the bulge region and their associated red GCs. Interestingly, at this stage, it has not been detected in the rich GC system of the massive elliptical M49 (Strader et al. 2006; Mieske et al. 2006a).

Given the evidence that extragalactic GCs are mostly old (Brodie & Strader 2006), the blue tilt implies a mass-metallicity relation for the metal-poor subpopulation of GCs (although this has yet to be confirmed spectroscopically). Various explanations have been proposed (see Bekki et al. 2007; Mieske et al. 2006a; Mieske 2009), but perhaps the most plausible explanation to date is one of self enrichment, whereby more massive GCs are enriched with more heavier metals during their brief formation period.

In the self enrichment models of Strader & Smith (2008) and Bailin & Harris (2009), a single generation of star formation and resulting supernovae is responsible for the self enrichment of each GC, which only becomes important above a threshold mass of $\sim 10^6 M_\odot$. Both models predict heavy element abundance variations within each massive GC, which may be the situation in some extragalactic GC systems (e.g.

* E-mail: dforbes@swin.edu.au

† Hubble Fellow

Cenarro et al. 2007). The Galactic GC system includes only a few GCs with masses $\geq 10^6 M_{\odot}$, so a clear signature of variation in colour (or metallicity) with magnitude (a blue tilt) is difficult to detect. It is thus important to determine whether galaxies similar to the Milky Way reveal a GC blue tilt or not.

Recently the ACS was used to study the star cluster system of the Sc galaxy NGC 3370 by Cantiello et al. (2009). NGC 3370 is a near face-on spiral at a somewhat larger distance of 28.7 Mpc. These two properties make it more difficult to study its GC system. Cantiello et al. detected 35 GC candidates with a mean colour $B-I = 1.60 \pm 0.27$ but no evidence of a blue tilt.

Here we present an analysis of the globular cluster system of NGC 5170 using the ACS camera on board the HST. NGC 5170 is a potential analogue of the Milky Way Galaxy with a Hubble type of Sb (Sandage & Bedke 1994) to Sc (NASA Extragalactic Database; NED). Fischer et al. (1990) derive a bulge-to-disk ratio of 0.5 which is more consistent with an Sb, like M31, than an Sc. It is a relatively isolated, edge-on ($i \sim 86^{\circ}$; Bottema et al. 1987) spiral with a total V band magnitude of 9.84 (NED). It lies at a Galactic latitude of 43° , making the surrounding field relatively free of Galactic stars and hence a good target for a GC study. A wide range of distance estimates are found in the literature. Ferrarese et al. (2000) report the GC luminosity function distance of Fischer et al. (1990) of 21.5 Mpc. However, Fischer et al. did not reach beyond the GC turnover magnitude so this value should be considered somewhat uncertain. The Tully-Fisher based distance estimates of Willick et al. (1997) range from 24 to 43 Mpc. The kinematic study of NGC 5170 by Bottema et al. (1987) assumed a distance of 20 Mpc. The Virgo infall corrected velocity (NGC 5170 lies behind but close to the Virgo cluster southern extension) from NED is $1665 \pm 27 \text{ km s}^{-1}$, which with $H_0 = 73 \pm 5 \text{ km s}^{-1} \text{ Mpc}^{-1}$ corresponds to a distance of $22.8 \pm 1.6 \text{ Mpc}$ ($m-M = 31.79 \pm 0.15$). The final error is the quadrature sum of the velocity error combined with the error on the Hubble constant. For this distance, the galaxy has an absolute magnitude of $M_V = -21.95$. We initially adopt this latter value, for which the pixel scale of the ACS ($0.05''$) equals $\sim 5 \text{ pc}$, but we reinvestigate this issue below and derive a new distance estimate based on measured sizes of the NGC 5170 GCs.

2 OBSERVATIONS AND DATA REDUCTION

The data for this work was taken using the ACS/WFC camera on board the HST as part of proposal ID 9766 (PI Forbes). Two pointings along the major axis of NGC 5170 were obtained in the F435W (B) and F814W (I) filters with a total exposure time of 3720s and 940s at each pointing. A ~ 500 pixel overlap between the two pointings gives a final area coverage of about $370'' \times 210''$. This corresponds to roughly $40 \text{ kpc} \times 23 \text{ kpc}$ (for an assumed distance of 22.8 Mpc), which would encompass over 90% of the Milky Way's GC system. The inter-chip gap region is projected along the disk of the galaxy.

Initial data reduction was carried out using the standard ACS calibration pipeline. Multiple exposures were aligned and combined using the multidrizzle task within IRAF. The profiles of common stars in the overlap region

were used to check the alignment process. The final two-pointing image is shown in Fig. 1.

3 GLOBULAR CLUSTER SELECTION AND PHOTOMETRY

Before the initial object detection, we subtracted a smooth model of the galaxy light from the image, using the ELLIPSE task in IRAF, to help with object detection and photometric analysis. DAOFIND was then used to select objects with a threshold 4 times the standard deviation of the background count level for both the B and I images.

An aperture magnitude was measured on all objects using an extraction radius of 5 pixels and a local background level estimated with a 5 pixel wide annulus starting at 20 pixels from the object.

The angular sizes of objects were determined with the latest version of the ISHAPE (Larsen 1999) program. We used empirical PSFs, which were constructed for the B and I band mosaics using ~ 30 point sources across the images. Point sources were identified as such using the FWHM calculated from a pass of SExtractor (Bertin & Arnouts 1996) over each mosaic. Isolated star-like objects with FWHM of 1.8–2.0 pixels (see Harris 2009a) were used to construct the empirical PSFs for ISHAPE with the standard DAOPHOT PSF software routine. Again following Harris (2009a), we used a King30 light profile with the default concentration parameter of $c = 1.5$ (King 1962). The ellipticity and position angle were allowed to vary during this fit. The final half light radii (r_h) were used to pick an appropriate aperture correction to derive total magnitudes following Harris (2009a).

Before converting the photometry to a standard photometric system, Galactic extinction corrections were applied using $E(B-V) = 0.08$ from the DIRBE dust maps (Schlegel et al. 1998) and extinction coefficients for a G1-star from Sirianni et al. (2005). No internal reddening correction is applied. Conversion of the total instrumental magnitudes to the standard Johnson B and I bands were carried out using the procedure of Sirianni et al. (2005) including colour terms. Charge transfer efficiency corrections are likely to be negligible in the bright galaxy halo regions of our detected objects, and were not applied. The B and I band objects were matched in position (with a 3 pixel tolerance) to create a common object list of sizes and extinction-corrected photometry.

Objects projected on the disk and inner bulge are very difficult to disentangle from star clusters and OB associations, and are problematic when it comes to measuring reliable photometry and sizes. We opted to apply a spatial cut to exclude the disk and inner bulge regions. This cut essentially removes a region above and below the (edge-on) disk. It means we may have partially selected against red (metal-rich) bulge/disk GCs that may be present, which preferentially lie in these regions.

As the distance to NGC 5170 is quite uncertain, we next applied a (distance-independent) colour selection. We selected only those objects with colours $1.2 < (B-I)_0 \leq 2.2$. Such a selection applied to the Milky Way would include over 95% of the GC system (Harris 1996).

Harris (2009a) has shown that objects with an ISHAPE

signal-to-noise ratio of less than 50, have unreliable size measures. Our data support this conclusion. We have therefore decided to select only those objects with an I band signal-to-noise ratio greater than 50. As shown in Fig. 2, the signal-to-noise ratio tracks the magnitude of an object, so that this selection cut is effectively a magnitude limit of $I \leq 23$ (which is a few tens of a magnitude brighter than the expected GC turnover magnitude, as discussed below). We note that the B band signal-to-noise ratio closely follows that of the I band (as the exposure times were chosen to give similar effective depths).

At this stage in our selection process, our object list contains several background galaxies. The next step in our selection criteria is to use the size as measured by ISHAPE as a means of excluding extended background sources and for identifying *bona fide* GCs.

The combination of high spatial resolution imaging from the ACS camera and the high Galactic latitude of NGC 5170 ensures that the contamination from foreground stars in our final object list is minimal. Nevertheless we applied a *minimum* size selection removing ~ 50 objects with half light sizes less than $0.01''$ as these are most likely stars (see Harris 2009a).

The half light sizes of GCs are thought to remain relatively stable as a GC evolves (Aarseth & Heggie 1998) and are found observationally to have a near constant average size in large galaxies (Jordan et al. 2005; Harris et al. 2009a). The latter suggests that comparison of the physical sizes of the objects in NGC 5170 with those of the Milky Way can be used to further refine our object list.

In Fig. 3 we show the size-magnitude distribution of objects assuming a Virgo-infall distance of 22.8 Mpc. The plot shows a fairly-well defined locus of objects in NGC 5170 with median sizes ~ 3.5 pc, which appear to have slightly larger sizes (and to be more luminous) than the bulk of the Milky Way GC system. A closer distance to NGC 5170 would provide better agreement between the two distributions. The brightest GC in the Milky Way, Omega Cen, with an extinction-corrected magnitude of $M_I = -11.2$ (and $(B-I)_o = 1.56$) is labelled. The second brightest is M54 with $M_I = -10.9$ (and $(B-I)_o = 1.61$). In Fig. 4 we show the same data but adjust the distance to NGC 5170 to be 19.5 Mpc (this choice of distance is justified below). Visually the two distributions appear better matched.

In an effort to create a cleaner sample (i.e. reduce the number of background galaxy contaminants) we imposed a size limit of $r_h < 0.05''$ (4.7 pc for a distance of 19.5 Mpc). The effect of this selection can be seen in Fig. 4. It shows that half a dozen Milky Way GCs (including Omega Cen) would be excluded, but the vast bulk remain. We note that the Milky Way GC system, and other galaxies, reveal a size versus galactocentric distance trend, such that the larger GCs tend to be located at large distances (van den Bergh et al. 1991; Jordan et al. 2005; Spitler et al. 2006; Gomez & Woodley 2007; Harris 2009b). The most distant selected object in our sample is at a projected radius of ~ 15 kpc, compared to the Milky Way GC system which extends to ~ 100 kpc. Thus a stricter size selection for NGC 5170 is probably justified.

Finally, we conducted a visual inspection of the selected objects. This was performed independently by two people (DF and JS). We attempted to identify objects that we

could confidently exclude as being non-GCs on the basis of their visual appearance. We identified 11 (DF) and 15 (JS) objects. There were 9 objects in common and these were generally classified as small galaxies. The different classifications tended to occur for the faint objects located near the galaxy disk, i.e. they may be reddened OB associations. We have chosen to exclude the combined list of 17 objects. The small number of visually excluded objects, several of which are at the faint end of our sample, do not affect our conclusions in terms of the colour-magnitude diagram, luminosity function or total population calculations. Our final object list contains 142 candidate GCs. Positions and photometry for these candidate GCs are listed in an on-line table.

The distance of 19.5 Mpc used above, was based on the empirical evidence that the average half light radius for GCs is relatively constant from system to system (Jordan et al. 2005; Harris et al. 2009a). To compare the NGC 5170 and Milky Way GC systems, we first restricted the Milky Way system to be only those GCs which have $M_I < -8.5$ (our effective magnitude limit) and we removed the large, outer GC NGC 2419 with a size of 17.9 pc. The remaining 56 GCs have a median half light radius of 3.12 pc with an error of ± 0.20 . The median half light radius for the final 142 NGC 5170 candidate GCs is $0.033'' \pm 0.001$. This angular size matches the Milky Way physical size for a distance of 19.5 ± 1.4 Mpc ($m-M = 31.45$). This value is within $\sim 2\sigma$ of the Hubble flow distance of 22.8 ± 1.6 Mpc. A histogram of the NGC 5170 candidate GCs (for a distance of 19.5 Mpc) compared to the Milky Way GC system is shown in Fig. 5. They have the same median half light size.

Fig. 6 shows the spatial distribution of the candidate GCs within our field-of-view of $\sim 28 \times 18$ kpc (for a distance of 19.5 Mpc). They are concentrated around the galaxy centre indicating that they are indeed associated with NGC 5170. Our spatial selection avoiding the region $\sim \pm 1$ kpc above and below the disk of the galaxy is clearly seen. A similar region in the Milky Way would exclude about 1/3 of the GCs and the vast bulk of starforming regions as the scale height for HII regions is ~ 50 pc (Paladini, Davies & de Zotti 2004). We found no significant trend in object size or magnitude with spatial location. The GCs located near to the galaxy bulge tend to have red colours, otherwise there is no strong colour dependence with spatial location. We have identified a possible Ultra Compact Dwarf (i.e. a GC-like object with a large size and high luminosity) as labelled in the figure. We discuss this UCD object in more detail in Section 6 below.

4 COLOUR-MAGNITUDE DIAGRAM

The observed colour-magnitude diagram for candidate GCs is shown in Fig. 7. We note that the location of objects in the colour-magnitude diagram is distance-independent. The colour-magnitude diagram reveals a concentration of blue objects with colour $(B-I)_o \sim 1.6$. Such colours are associated with the metal-poor subpopulation of GCs (e.g. Barmby et al. 2000). It can be seen that the general locus of this blue subpopulation for $I \leq 22$ tends to have redder colours at brighter magnitudes; i.e. a blue tilt. The metal-rich subpopulation is expected at $(B-I)_o \sim 1.9$. There are a few objects with such colours, but as noted earlier we partially selected

against bulge/disk GCs which comprise the metal-rich GC subpopulation in spirals. Within our defined field-of-view, and assuming a blue/red colour division at $(B-I)_o \sim 1.75$, we find the fraction of red-to-blue GCs to be 0.29. Extending to larger galactocentric radii would tend to decrease this fraction, while accounting for missing bulge/disk GCs would tend to increase it. However, assuming a spatial distribution similar to the Milky Way's GC system, this fraction will be largely unchanged at 1/3.

In an attempt to quantify the visual trend for the blue subpopulation to become redder with increasing brightness, we have used the NMIX statistical test (see for example Spitler et al. 2006). We divide the sample at $I = 22$, which corresponds to roughly half of the sample in number. For the brighter half, we find 42 (63%) of the GCs are assigned to the blue subpopulation with a mean colour, rms dispersion and error on the mean $(B-I)_o = 1.580 \pm 0.101$ (0.016) and 24 (37%) are red with values of $(B-I)_o = 1.828 \pm 0.151$ (0.031). For the fainter half, the blue/red fractions are similar at 53 (70%) to 23 (30%). However the mean colour, rms dispersion and error on the mean are now $(B-I)_o = 1.516 \pm 0.115$ (0.016) and 1.771 ± 0.172 (0.036). Thus there is a marginal 2σ difference in the mean colour of the red subpopulation with magnitude but the bright blue GCs are redder than the faint blue ones at the $\sim 3\sigma$ level. In Fig. 7 we overlay the mean value, error on the mean and the rms dispersion for the blue subpopulation. The colour difference is $\Delta(B-I)_o = 0.064 \pm 0.02$. If we assume a linear transformation from colour to metallicity of the form $\Delta(B-I)/\Delta[\text{Fe}/\text{H}] = 0.375$ (Harris et al. 2006), then this translates into $Z \sim L^{0.42 \pm 0.13}$. A further division into three magnitudes bins supports the colour-magnitude trend of the blue subpopulation but with lower significance. Thus we confirm the visual trend in Fig. 7 of colour bimodality with a blue tilt and no strong evidence of a red tilt. We note that the appearance of the blue tilt does not depend strongly on the exact choice of a maximum size criterion nor on the region excluded above and below the disk.

In Fig. 8 we show the colour-absolute magnitude diagram for a distance of 19.5 Mpc ($m-M = 31.45$). The universal peak of the GC luminosity function occurs at $M_I \sim -8.3$, which is fainter than the cutoff magnitude of our data. Thus if this is the true distance, we can not use our observed GC luminosity function to accurately determine the distance.

Fig. 8 also shows a comparison to the well-defined blue tilt of Harris (2009a) who used a composite GC system from several massive early-type galaxies. The data were also taken in the B and I bands with the ACS camera. We show the mean values of the blue and red GC subpopulations and his 2nd order polynomial fit to the blue subpopulation. Although they extend to higher luminosities, the blue tilt observed in these massive early-type galaxies appears to be similar to that seen in NGC 5170 for the range $-9.5 > M_I > -11$, scattering evenly about the Harris fit line. Harris (2009a) quotes the mass-metallicity relation for a simple linear fit to the massive early-type galaxies of $Z \sim L^{0.48 \pm 0.12}$. This is consistent with that found for NGC 5170 candidate GCs (over a more limited magnitude range).

There is an indication that the metal-rich GCs NGC 5170 are slightly bluer (more metal-poor) on average than those in the massive ellipticals. This is to be expected given the correlation of the mean colour of the red subpopula-

tion with host galaxy luminosity (Forbes, Brodie & Grillmair 1997; Brodie & Strader 2006).

A comparison to the Milky Way GC system is given in Fig. 9. To our cutoff magnitude of $M_I \sim -8.5$, the two distributions are similar in form despite the fact that extinction corrections for some Milky Way GCs can be quite uncertain. This figure also clearly shows that there are more candidate GCs associated with NGC 5170 than the Milky Way. This includes the red subpopulation, for which we are incomplete at all magnitudes.

In Fig. 10 we reproduce the NGC 5170 GC colour-absolute magnitude diagram again, but with a simulated GC system added. Here we have used the self enrichment model of Bailin & Harris (2009) to generate a distribution of model GCs as described in Harris et al. (2009a), incorporating early self enrichment plus later dynamical mass loss. The blue subpopulation was assumed to have a mean metallicity $[\text{m}/\text{H}] = -1.6$ and the red ones with $[\text{m}/\text{H}] = -0.7$. Each sequence was assigned an internal metallicity spread of ± 0.35 dex. In the figure, we show the resulting mean and rms dispersion of the simulated metal-poor and metal-rich GCs for these input values. The blue tilt is apparent in the simulated data for bright magnitudes. For a linear mass-metallicity relation fit to all four mean values, the resulting relation has the form $Z \sim L^{0.54 \pm 0.07}$. This is consistent with that found for the NGC 5170 candidate GCs. Fig. 10 also shows the mean colours of the blue subpopulation in NGC 5170. We note that the Bailin & Harris (2009) model also captures, to first order, the main features of the colour-magnitude diagram of the Sombrero galaxy GCs (Harris et al. 2009a) and GCs in other massive ellipticals (Wehner et al. 2008; Harris 2009b).

5 ESTIMATING THE TOTAL GC SYSTEM POPULATION

5.1 Spatial Distribution

We follow the method of Kissler-Patig et al. (1999) and Harris et al. (2009b) to estimate our spatial coverage of the NGC 5170 GC system. This method assumes that the Milky Way and NGC 5170 GCs have a similar spatial distribution. Globular clusters within 1 kpc of the Milky Way centre were excluded and the Y (parallel) and Z (perpendicular) coordinates were then projected onto our search area. We found 70 out of 150 GCs in the catalogue of Harris (1996) are contained in our search area. Thus spatially we detect almost half of the total GC system.

If NGC 5170 were located at a distance 10% further (closer) then the number found would decrease (increase) by about 4 (3%) GCs. The change in the number of GCs is relatively insensitive to distance as any increase in the area of the halo searched is compensated for by the size of the disk region that is excluded.

5.2 Completeness Tests

In order to estimate the magnitude completeness of our sample, we added simulated point sources to the B and I band ACS images (the actual GCs in NGC 5170 are partially resolved with half light sizes of ≤ 1 pixel). These simulated

sources were fully calibrated onto the standard Johnson photometric system in a similar manner to the actual GC candidates with an intrinsic colour of $B-I = 1.7$ imposed. We ensured that none of the simulated sources were placed near GC candidates and we avoided the disk region but otherwise sources were distributed at random on the image. We used DAOFIND with the same detection parameters to recover the simulated sources. Our tests suggest that we are 100% complete at our cutoff magnitude of $I \sim 23$. This corresponds to $M_I \sim -8.5$, and hence we have not quite reached the expected GC luminosity function turnoff at $M_I \sim -8.3$. In other words, we have detected slightly less than half of the GC system in terms of magnitude.

5.3 Number of GCs and Specific Frequency

As stated above, we expect contamination from foreground stars in our final object list to be minimal. As the surface density of objects declines with galactocentric distance, and our spatial coverage is a fraction of the Milky Way GC system extent, the number of unresolved background galaxies with colours matching those of GCs is likely to be very small. From our visual inspection of the images, we suspect that the main source of any contamination is misclassified star-forming regions (combined with some internal reddening to produce colours similar to a GC) located close to the galaxy disk. If as many as half of the 26 objects with $1 < |Z| < 2$ kpc of the galaxy disk are actually star-forming regions, then the resulting uncertainty on our final object list of 142 is 9%. This gives a first order estimate of the uncertainty associated with misclassified star-forming regions.

It is also possible that *bona fide* GCs have been reddened sufficiently by internal dust so as to shift their colours beyond our red limit, i.e. $(B-I)_o > 2.2$. However the small relative number of red ($(B-I)_o \sim 1.9$) GCs that we detect suggests that reddening of intrinsically blue GCs is a minor effect.

In order to calculate the total GC system of NGC 5170, we require a factor of two correction in both spatial area and luminosity (with an estimated 10% uncertainty on each). Adding the various uncertainties in quadrature gives a total error of 17%. Our estimate for the total GC system for NGC 5170 is 600 ± 100 . An additional source of uncertainty in this estimate is the distance to NGC 5170, which strongly affects the magnitude incompleteness correction. If the galaxy is actually at a larger distance (as suggested by the Tully-Fisher measurements of Willick et al. 1997) then our estimate of the total number of GCs would be an upper limit. For a distance of 19.5 Mpc and $M_V = -21.6$, we calculate a specific frequency of $S_N = 1.37 \pm 0.23$. This can be compared to the GC system numbers derived by Fischer et al. (1990) of 815 ± 320 and $S_N = 1.3$ for an assumed distance of 31.6 Mpc and $M_V = -22.0$.

6 A POSSIBLE ULTRA COMPACT DWARF

Our ACS imaging field includes a bright object which is excluded from our final GC list. Its magnitude $I_o = 19.00$ and its size of $0.065''$ (in both B and I filters) corresponds to are $M_I = -12.45$ and $r_h = 6.14$ pc for a distance of 19.5 Mpc. It has a relatively red colour $(B-I)_o = 1.89$ and it appears

quite round in the ACS images. It is located at R.A. = 13:29:53.4 and Dec. = -17:59:09.1 (J2000), SE of the galaxy disk (see Figures 1 and 5). A recession velocity is needed to confirm its association with NGC 5170.

Whether this object should be classified as a massive GC or an Ultra Compact Dwarf is a matter of debate. The properties of objects classified as UCDs overlap with those that have been classified as massive GCs (e.g. Forbes et al. 2008). Indeed the properties of the object described above lie within the range of those found for GCs in the rich GC systems studied by Harris (2009a). So although the object is clearly distinct from the bulk of the NGC 5170 GCs in terms of its luminosity, it is still consistent with being drawn from a (universal) GC luminosity function. Mieske et al. (2006b) have suggested that a GC/UCD transition occurs at $M_V \sim -11$ ($M_I \sim -12$) or a few million solar masses, as this marks the change from a near constant size to one that scales with luminosity. (Mieske et al. 2006b; Forbes et al. 2008). By this definition, the NGC 5170 object would be classified as a UCD.

7 DISCUSSION AND CONCLUSIONS

Using two pointings of the HST/ACS camera, in the B and I filters, we have explored the GC system surrounding the edge-on spiral galaxy NGC 5170. We employed the aperture-correction method of Harris (2009a) for partially resolved objects to obtain accurate total magnitudes. The initial selection of candidate GCs is based on $(B-I)_o$ colour and signal-to-noise ratio (which closely tracks magnitude). We used the object size, as measured by ISHAPE, to further refine the selection process and to provide an estimate of the distance to NGC 5170 (under the assumption of a universal average size for GCs). This distance is 19.5 Mpc and is within $\sim 2\sigma$ of the Hubble flow distance.

The colour-magnitude diagram reveals a well-populated blue subpopulation and a sparse red subpopulation, in a ratio of roughly 3 to 1. The GC subpopulation colours are similar to those seen in the Milky Way and M31 GC systems. We also find a blue tilt that is similar, within our restricted magnitude range, to that for massive ellipticals found by Harris (2009a) and to the self enrichment model described in Harris et al. (2009a). These findings suggest that normal late-type spiral galaxies, along with galaxies of earlier types, host GC systems with a blue tilt. The blue tilts are most likely evidence for a mass-metallicity relation within the metal-poor GC subpopulation. The reason for the lack of an observed blue tilt in the Milky Way GC system appears to be simply due to the small number of relatively massive GCs (Bailin & Harris 2009; Harris 2009a). We would expect that new, high precision photometry of a large sample of the M31 GC system should reveal a blue tilt.

We note that the reality of blue tilts in general has been disputed by Kundu (2008), and in the case of M87 in particular by Waters et al. (2009). Subsequent work by Harris (2009a,b), Peng et al. (2009) and Madrid et al. (2009) has addressed the issues raised by these workers and has strongly confirmed the astrophysical reality of blue tilts.

Although of similar Hubble type and total magnitude to the Milky Way (Sbc, $M_V \sim -21.3$), we find that the GC system of NGC 5170 is much richer with a total GC pop-

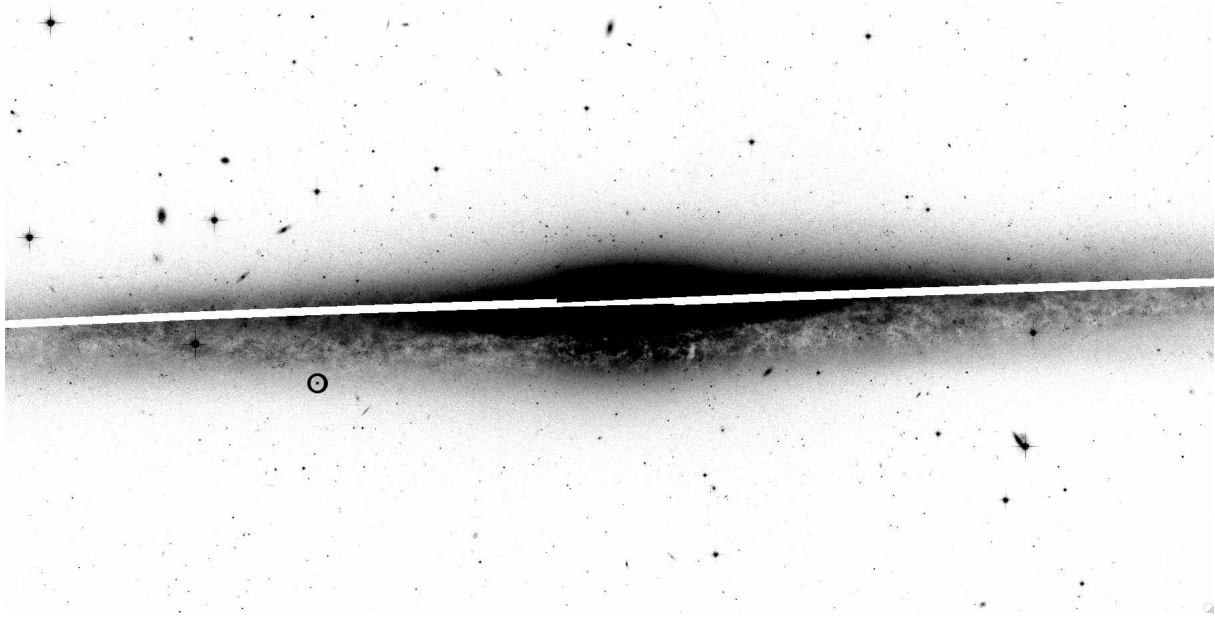


Figure 1. HST/ACS I band image of NGC 5170 covering $370'' \times 210''$. North is up and East is left. The inter-chip gap runs across the image East-West. The location of a potential Ultra Compact Dwarf is shown by an open circle.

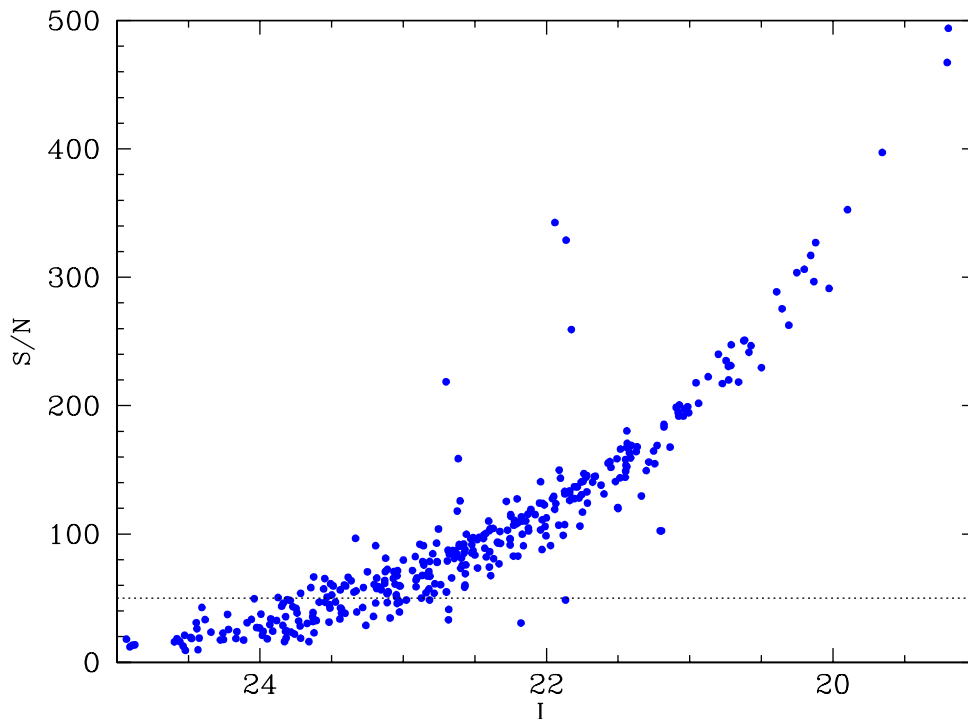


Figure 2. I band signal-to-noise ratio as a function of I magnitude. A signal-to-noise cut of greater than 50 (shown by the horizontal line) is adopted for object selection.

ulation of 600 ± 100 GCs. In this sense NGC 5170 bears more resemblance to the Sb galaxy M31 with ~ 450 GCs (Barmby et al. 2000), or the Sa Sombrero galaxy with 1900 GCs (Rhode & Zepf 2004).

A commonly-used measure to directly compare GC systems is the specific frequency S_N , which normalises GC num-

ber by M_V . Assuming $M_V = -21.6$ for NGC 5170, we estimate $S_N = 1.37 \pm 0.23$. This is higher than the Local Group spirals (i.e. for the Milky Way $S_N = 0.6$ and M31 $S_N = 0.9$) and the four Sb-Sc spirals studied by Rhode et al. (2007) who found a range of $0.5 < S_N < 0.9$, but less than $S_N = 2.1$ for the Sombrero galaxy (Rhode & Zepf 2004). An alter-

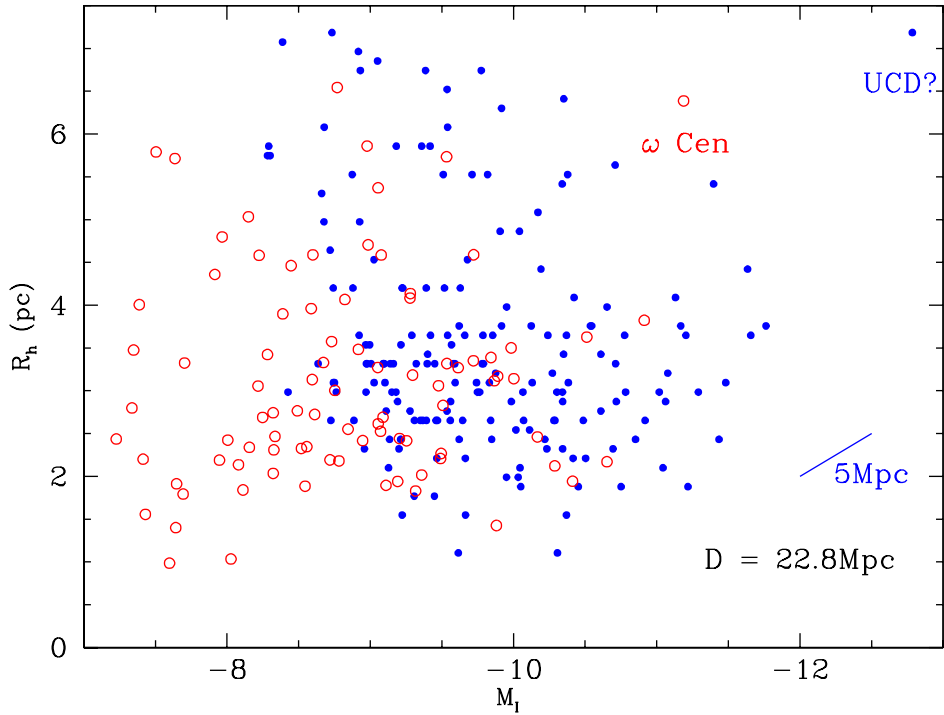


Figure 3. Half light radius vs extinction-corrected I band absolute magnitude for NGC 5170 candidate GCs (blue filled circles) compared to Milky Way GCs (red open circles). A distance of 22.8 Mpc is assumed. The length and angle of the solid line indicates the effect of a change of 5 Mpc in distance to NGC 5170. The location of Omega Cen and the possible Ultra Compact Dwarf around NGC 5170 are labelled. The locus of NGC 5170 objects is offset from that of the Milky Way GCs.

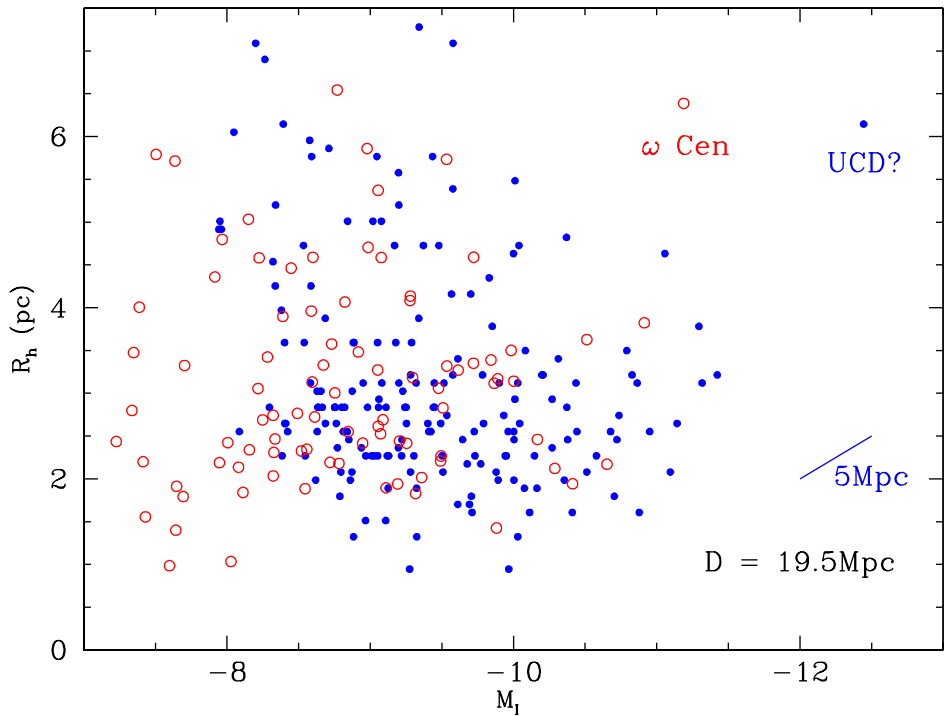


Figure 4. Half-light radius vs extinction-corrected I band absolute magnitude for NGC 5170 candidate GCs compared to Milky Way GCs. A distance of 19.5 Mpc is assumed. Other labels as per Fig. 3. The locus of NGC 5170 objects is similar to the Milky Way size-magnitude distribution for a distance of 19.5 Mpc.

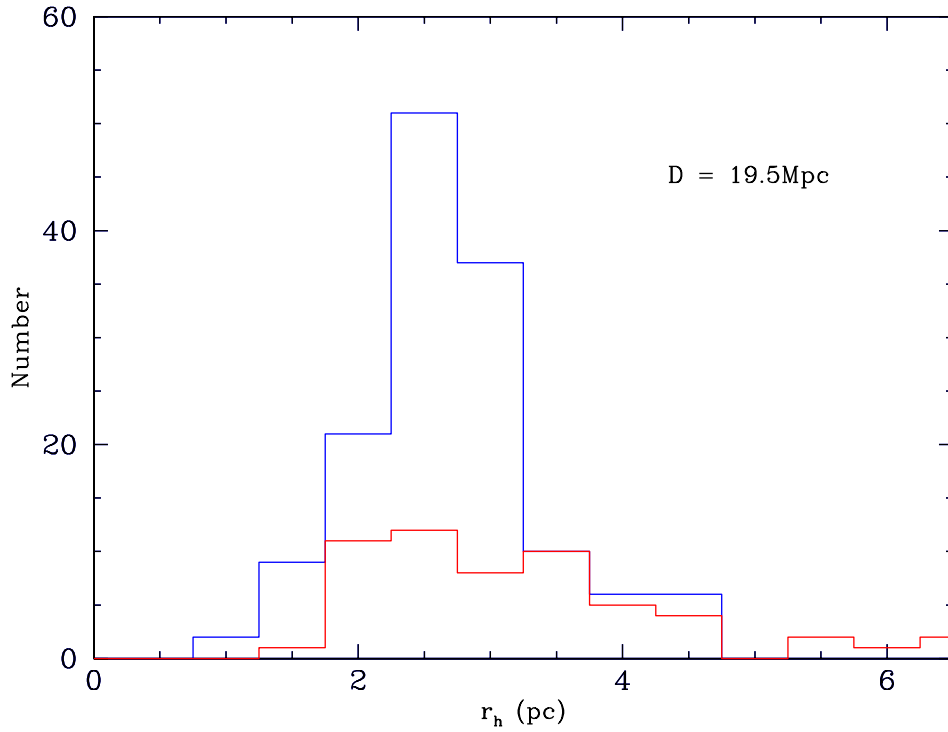


Figure 5. Histogram of half-light radius. The upper blue histogram shows the NGC 5170 candidate GCs, while the lower red histogram shows the Milky Way GC system restricted to $M_I < -8.5$. A distance of 19.5 Mpc is assumed. The two distributions have the same median half light radius.

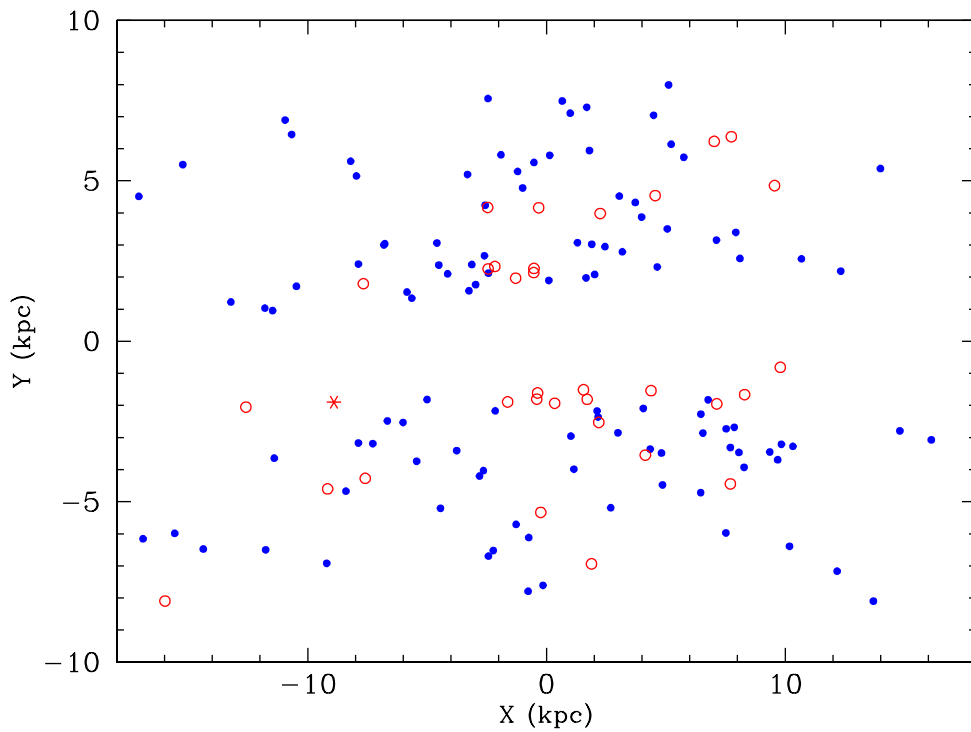


Figure 6. Spatial location of GC candidates around NGC 5170. The bulge and disk regions have been excluded from the selection process. Blue GCs ($B-I < 1.75$) are shown by blue filled circles, and red GCs by red open circles. The location of the possible Ultra Compact Dwarf is shown with a red star symbol. A distance of 19.5 Mpc is assumed.

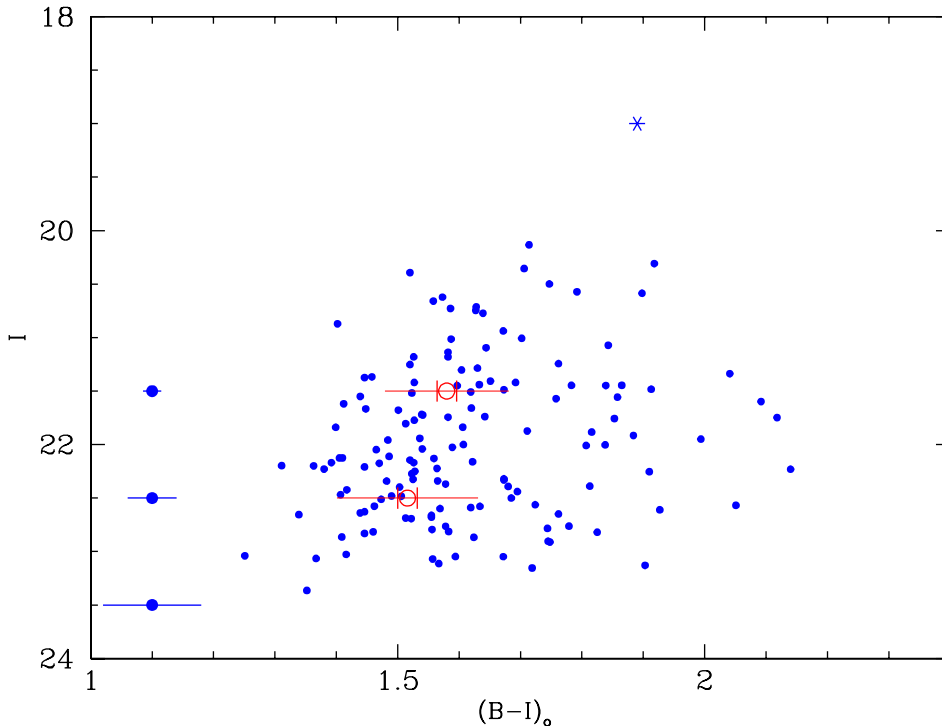


Figure 7. Observed colour-magnitude diagram for NGC 5170 candidate GCs. The mean value (open circle), error on the mean (vertical tick) and rms dispersion (horizontal line) for the blue subpopulation from the NMIX statistical test are overlaid. A colour difference is seen, at the $\sim 3\sigma$ level, between the blue GCs brighter/fainter than $I = 22$, i.e. a blue tilt. The red ($B-I \sim 1.9$) subpopulation is sparse as we have partially selected against bulge/disk GCs.

native measure for comparing GC systems is the stellar mass normalised GC frequency, T_N (Rhode & Zepf 2004; Spitler et al. 2008). Using the 2MASS K band magnitude of 7.63 and a Salpeter IMF we derive a stellar mass of $7.6 \times 10^{10} M_\odot$. This gives $T_N \sim 8$. However this likely an upper limit given that some fraction of the K band flux will be obscured due to the highly edge-on ($i \sim 86^\circ$) nature of NGC 5170. Spitler et al. showed that T_N varies with the stellar mass of the host, and that the Sombrero galaxy had the highest T_N value (~ 9) of the 8 spiral galaxies listed. Thus NGC 5170 appears to have a high GC frequency, placing it between the Local Group spirals and the Sombrero galaxy.

Using the scaling relation of Spitler & Forbes (2009) between total GC system mass with halo mass, we estimate a halo mass for NGC 5170 to be $3.4 \times 10^{12} M_\odot$. This is a factor of 2-3 \times that of the Milky Way halo mass.

We also report the discovery of a possible Ultra Compact Dwarf associated with NGC 5170. If confirmed by its radial velocity, it will be another rare example of a UCD located near a spiral galaxy outside that of a galaxy cluster (see Hau et al. 2009).

ACKNOWLEDGMENTS

We would like to thank K. Forde for his work performing the initial data reduction. DF and LS thanks the ARC for financial support. We thank C. Foster for useful comments on this work. This material is based upon work supported by NSF grant AST-0507729. We acknowledge the usage of

HyperLeda and NED databases. Finally, we thank the referee for several useful suggestions that have improved the paper.

REFERENCES

- Aarseth S. J., Heggie D. C., 1998, MNRAS, 297, 794
- Bailin J., Harris W. E., 2009, ApJ, 695, 1082
- Barmby P., Huchra J. P., Brodie J. P., Forbes D. A., Schroder L. L., Grillmair C. J., 2000, AJ, 119, 727
- Bekki K., Yahagi H., Forbes D. A., 2007, MNRAS, 377, 215
- Bertin E., Arnouts S., 1996, A&AS, 117, 393
- Bottema R., van der Kruit, P., Freeman K., 1987, A&A, 178, 77
- Brodie J. P., Strader J., 2006, ARA&A, 44, 193
- Cantiello M., Brocato E., Blakeslee J., 2009, 0906.3432
- Cenarro A. J., Beasley M. A., Strader J., Brodie J. P., Forbes D. A., 2007, AJ, 134, 391
- Ferrarese L., et al., 2000, ApJS, 128, 431
- Fischer P., Hesser J. E., Harris H. C., Bothun G. D., 1990, PASP, 102, 5
- Forbes D. A., Brodie J. P., Grillmair C. J., 1997, AJ, 113, 1652
- Forbes D. A., Lasky P., Graham A., Spitler L.R., 2008, MNRAS, 389, 1924
- Gómez M., Woodley K. A., 2007, ApJ, 670, L105
- Goudfrooij P., Strader J., Brenneman L., Kissler-Patig M., Minniti D., Edwin Huizinga J., 2003, MNRAS, 343,

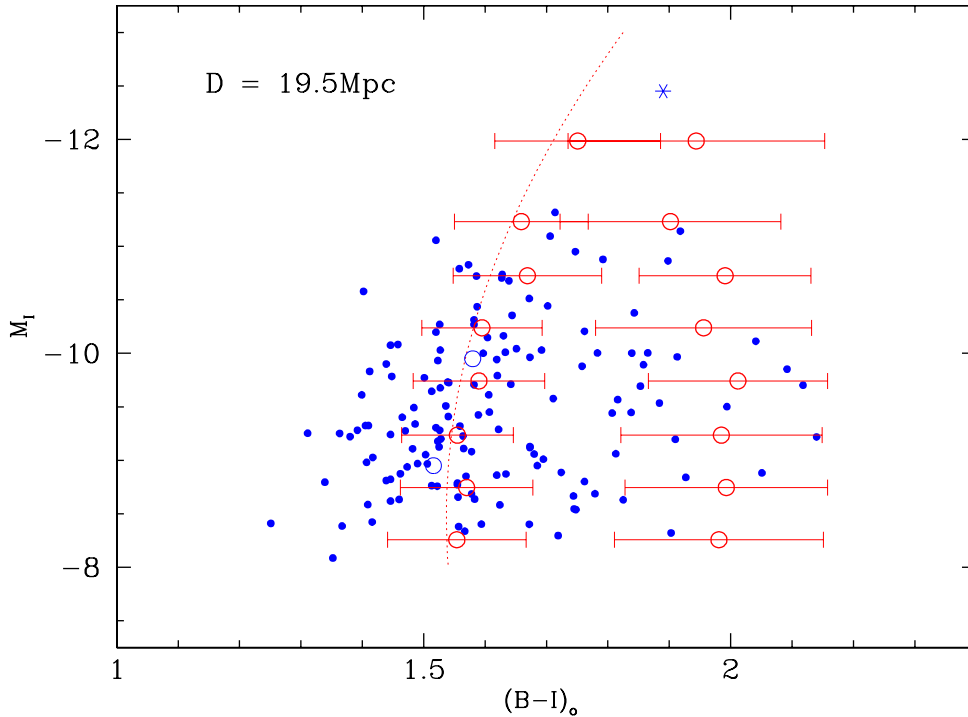


Figure 8. Colour-absolute magnitude diagram for NGC 5170 candidate GCs (assuming a distance of 19.5 Mpc). Also included is the potential UCD, given by a star symbol. Red open circles and error bars represent the mean values and rms dispersions for the combined sample of massive ellipticals from Harris (2009a). A 2nd order polynomial fit to the massive elliptical data is given by a dashed line. Blue open circles without error bars are the mean values for the NGC 5170 blue GC subpopulation. In the Milky Way, Omega Cen has $M_I = -11.2$ and the (universal) GC luminosity function turnover is at $M_I \sim -8.3$. The blue subpopulation in NGC 5170 is consistent with the blue tilt seen in the massive ellipticals but covers a much smaller magnitude range with fewer GCs.

665

Harris W. E., 1996, *AJ*, 112, 1487
Harris W. E., Whitmore B. C., Karakla D., Okoń W., Baum W. A., Hanes D. A., Kavelaars J. J., 2006, *ApJ*, 636, 90
Harris W. E., 2009a, *ApJ*, 699, 254
Harris W. E., 2009b, *ApJ*, 703, 939
Harris W. E., Spitler L. R., Forbes D. A., Bailin J., 2009a, *MNRAS*, submitted
Harris W. E., Mouhcine M., Rejkuba M., Ibata R., 2009b, *MNRAS*, 395, 436
Hau G., Spitler L., Forbes D., Proctor R., Strader J., Mendel J., Brodie J., Harris W., 2009, *MNRAS*, 0901.0639
King I., 1962, *AJ*, 67, 471
Kissler-Patig M., Ashman K. M., Zepf S. E., Freeman K. C., 1999, *AJ*, 118, 197
Kundu A., 2008, *AJ*, 136, 1013
Jordán A., et al., 2005, *ApJ*, 634, 1002
Larsen S. S., 1999, *A&AS*, 139, 393
Madrid J., Harris W., Blakeslee J., Gomez M., 2009, 0909.0272
Mieske S., et al., 2006a, *ApJ*, 653, 193
Mieske S., et al., 2006b, *AJ*, 131, 2442
Mieske S., 2009, *Globular Clusters: Guides to Galaxies*, T. Richtler and S. Larsen, ESO Astrophysics Symposia, Springer
Paladini R., Davies R., de Zotti G., 2004, *MNRAS*, 347, 237

Peng E. W., et al., 2009, *ApJ*, 703, 42
Rhode K., Zepf S., Kundu A., Larner A., 2007, *AJ*, 134, 1403
Sandage A., Bedke J., 1994, *The Carnegie Atlas of Galaxies*. Carnegie Inst. Wash. Publ.
Schlegel D. J., Finkbeiner D. P., Davis M., 1998, *ApJ*, 500, 525
Sirianni M., et al., 2005, *PASP*, 117, 1049
Spitler L. R., Larsen S. S., Strader J., Brodie J. P., Forbes D. A., Beasley M. A., 2006, *AJ*, 132, 1593
Spitler L. R., Forbes D. A., Strader J., Brodie J. P., Gallagher J. S., 2008, *MNRAS*, 385, 361
Spitler L. R., Forbes D. A., 2009, *MNRAS*, 392, 1
Strader J., Brodie J. P., Spitler L., Beasley M. A., 2006, *AJ*, 132, 2333
Strader J., Smith G. H., 2008, *AJ*, 136, 1828
van den Bergh S., Morbey C., Pazder J., 1991, *ApJ*, 375, 594
Waters C. Z., Zepf S. E., Lauer T. R., Baltz E. A., 2009, *ApJ*, 693, 463
Wehner E. M. H., Harris W. E., Whitmore B. C., Rothberg B., Woodley K. A., 2008, *ApJ*, 681, 1233
Willick J. A., Courteau S., Faber S. M., Burstein D., Dekel A., Strauss M. A., 1997, *ApJS*, 109, 333

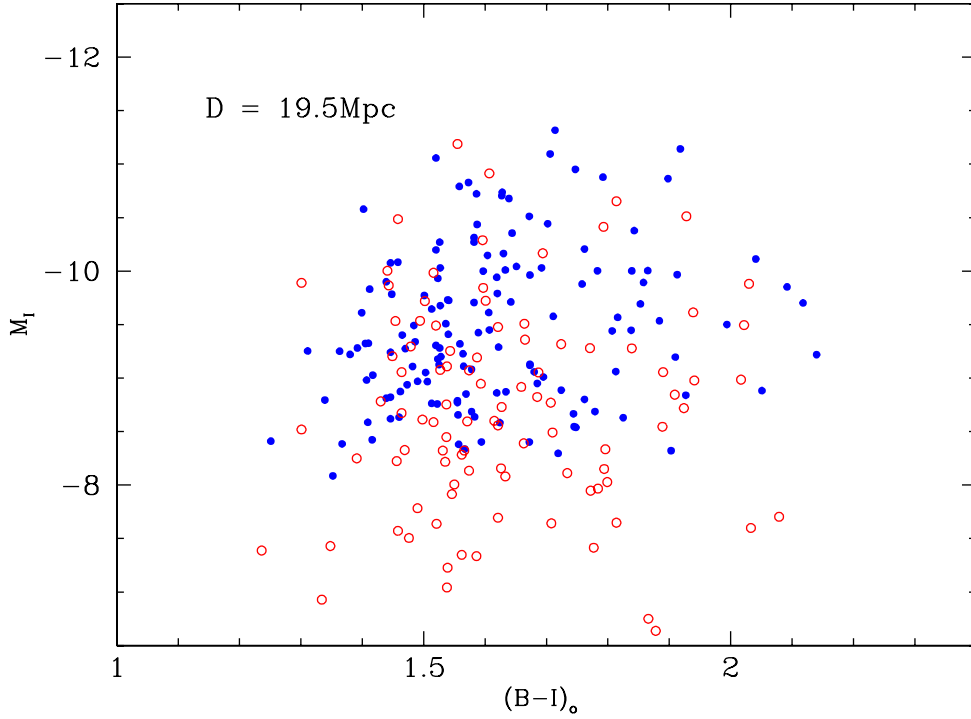


Figure 9. Colour-absolute magnitude diagram showing NGC 5170 candidate GCs (blue filled circles) and Milky Way GCs (red open circles). The colour-magnitude distributions are similar for the two GC systems, although NGC 5170 clearly includes more objects brighter than our cutoff magnitude of $M_I \sim -8.5$.

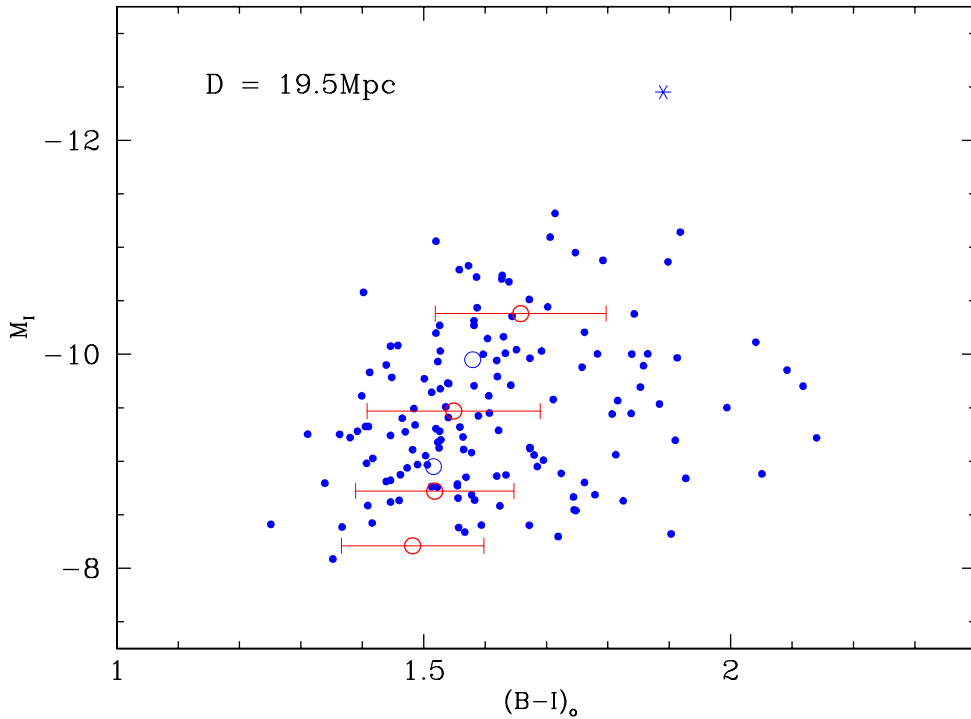


Figure 10. Colour-absolute magnitude diagram showing NGC 5170 candidate GCs (small blue circles) with mean values and rms dispersion for the simulated data (large red circles with error bars). Blue open circles without error bars are the mean values for the NGC 5170 blue GC subpopulation. Also included is the potential UCD, given by a star symbol. The simulated data are generated from the self enrichment model, which includes dynamical mass loss, as described in Harris et al. (2009a).